ACTA ACUSTICA UNITED WITH ACUSTICA
Vol. 88 (2002) 970 – 985

On the Creation of the Helmholtz Motion in Bowed Strings

Knut Guettler
Norwegian Academy of Music, P.B. 5190 Majorstuen, N-0302 Oslo, Norway. knut.guettler@nmh.no

Summary
In this study, the conditions for establishing Helmholtz motion in a bowed string are studied analytically and by computer simulations. For simple models of the bowed string, the bow force and bow acceleration are the two operative parameters during the creation of the Helmholtz motion. Parameter spaces for bow force and bow acceleration during the build-up of a regular Helmholtz motion are computed. These spaces have triangular shape in the initial part of the transient. Similar results are observed with more advanced simulation models.
PACS no. 43.75.De

1. Introduction

The steady-state dynamics of a bowed string oscillating in Helmholtz motion seems in many respects well analysed and understood. The creation of the Helmholtz motion, however, has not been subject to equally comprehensive analyses, in spite of its relevance for the player. The works by Schelleng [1, 2] describe the criteria for maintaining a steady Helmholtz motion in a bowed string. Given the bowing position, the characteristic wave resistance of the string, and the impedances of the string terminations, the *bow force* ("bow pressure"), and *bow velocity* constitute the two control parameters of the string motion. During the creation of the Helmholtz motion, however, the *bow force* and *bow acceleration* are the two operative parameters, as shown in this study. If a proper Helmholtz motion, and thus a full tone, is to be quickly established, these two control parameters must be kept within certain limits. If not, a periodical slip-stick triggering is not likely to develop during the first few periods.

2. The Helmholtz motion in steady state

Figure 1 shows the behaviour of a simple model of a bowed string in steady-state Helmholtz motion. For almost the entire period, the friction force between bow and string stays nearly constant, with the exception of some small ripples. Only once a period, when the sum of the velocity waves returning from the bridge and nut suddenly takes a high magnitude with a direction opposite to that of the bow velocity, the friction force will rise and form a spike. This force spike must reach the limiting static friction force before a string release can take place. For the discussion on the creation of the Helmholtz motion to follow, it is important to notice the features of the velocity waves returning to the bow after reflections at the bridge and nut, respectively: In the d'Alembert solution to the wave equation (see Appendix A1), with a rational bowing position, the Helmholtz motion gives a stepwise *descending* velocity signal returning from the bridge, and a stepwise *ascending* signal returning from the nut (relative to a positive bow velocity). As will be shown, the reflections from the bridge will build up a descending velocity signal as soon as the bow starts pulling the string out of equilibrium. The remaining task in the creation of a regular Helmholtz motion is simply to achieve a periodic pattern of reflected velocity pulses from the nut with *increasing* magnitudes in the course of the transient.

The simulations shown in Figure 1 are based on a relatively unsophisticated model, giving a clean and simple sketch of some basic features during steady-state Helmholtz motion. In particular, the steps of the returning waves are clearly visible. Some rounding of the steps takes place, due to frequency-dependent losses in the reflection functions for the bridge and nut. Higher modes are heavily damped by modelling the bridge and nut terminations with stiffness, and resistances matching that of the string. In order to maintain the steady-state oscillation, lost energy has to be replaced during every cycle, which leads to the small ripples seen in the friction force during stick. More realistic loss parameters would have given a more "nervous" picture, to which also string torsion, due to the bow's tangential excitation, would have contributed considerably.

During the last years, many characteristic features have been included in the simulations of the bowed string, increasingly adding to the degree of realism. String torsion [3], reflection functions including string stiffness [4], finite width of bow hair ribbon [5], bow resonances [6], and "plastic" friction characteristics [7], are examples of important advancements in modelling.

Received 31 October 2001,
accepted 6 May 2002.

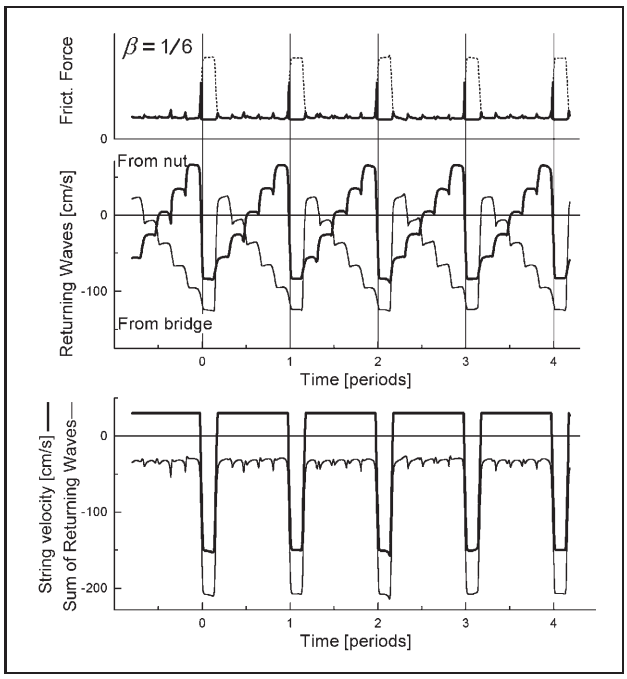

Figure 1. Simulation of the Helmholtz motion in steady state. Upper panel: Friction force (thick line); "potential friction force" (thin line), i.e. the force that would be acting on the bow if the limiting static frictional force were instantly raised to a sufficiently high level (see Appendix A2). Middle panel: Velocity waves returning from the bridge (thin line) and nut (thick line). Lower panel: String velocity at the point of bowing (thick line); sum of the velocity waves returning from the bridge and nut (thin line). Bow speed 30 cm/s; relative bowing position $\beta = 1/6$. Compliant string terminations with resistances matching the wave resistance of the string. "Hyperbolic" friction characteristic (see Figure 15).

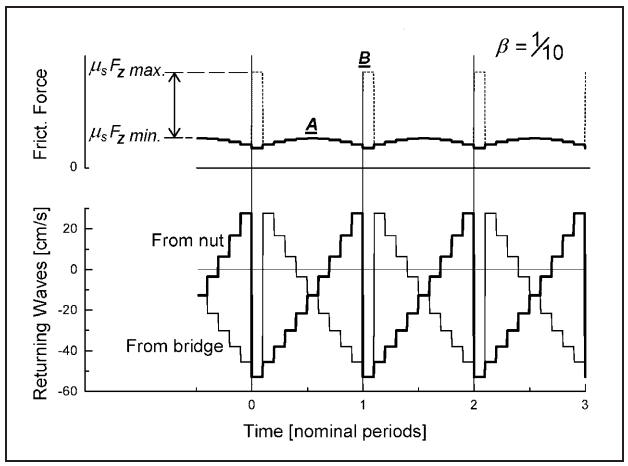

Figure 2. Simulation of forces and velocity wave patterns in a model with purely resistive string terminations (Raman model). These graphs illustrate the waveforms upon which Schelleng based his analysis of bow-force limits. Upper panel: Friction force (thick line); "potential friction force" (dotted line). Lower panel: Velocity waves returning from the bridge (thin line) and nut (thick line). The string is slipping through the first tenth of each nominal period, during which time interval the friction force is equal to $\mu_d F_Z$. The points indicated by ***A*** and ***B*** are the critical moments for determining the lower and upper limits in bow force, respectively (see text) (Relative bowing position $\beta = 1/10$. Reflection functions at bridge and nut: $\lambda_{BRG} = \lambda_{NUT} = 0.95$, "hyperbolic" friction characteristics).

Schelleng's analysis of the Helmholtz motion [1] was based on an even simpler model than that in Figure 1, suggested by Raman [8]. By defining the string terminations as purely resistive (or dominated by resistance), one may model the reflection coefficient as a real fraction: $\lambda = (R-Z)/(R+Z)$, where R and Z are the bridge resistance and the characteristic wave resistance of the string, respectively. Figure 2 shows Schelleng's method of analysis. The friction force undergoes a cycle for each fundamental period. Let us term the bowing position relative to the string length β. In cases where $1/\beta$ is an integer, the friction force will reach maximum magnitude in the middle of the stick interval (disregarding the spike in friction force initiating the transition from stick to slip). The moment of this force maximum is marked ***A*** in the figure. This point defines a *lower limit* in bow force for the given combination of bowing speed and bow position: If the limiting static frictional force is not equal to or higher than the friction force at ***A***, the string will make a (second) slip at this point. At the other extreme, an *upper limit* in bow force is defined by the friction force at point ***B***, the nominal moment of release. If the limiting static frictional force exceeds the value of the "potential frictional force" at this point, a regular slip will not be triggered as the Helmholtz kink passes under the bow. The "potential friction force" is a useful quantity, defined as the force that would be acting on the bow due to the combined effects of bow velocity and velocity waves returning from the bridge and nut, provided that the limiting static frictional force was sufficiently high to keep the string sticking (see Appendix A2).

On basis of the periodic rise in static friction force above the dynamic (sliding) friction, Schelleng calculated the requirements for maintaining the Helmholtz motion to be (here quoted in condensed form)

$$\frac{(\mu_s - \mu_d)\beta}{Z} \leq \frac{v_b}{F_Z} \leq \frac{2(\mu_s - \mu_d)\beta^2 R}{Z^2}, \qquad (1)$$

$(\beta \geq Z/2R)$, where μ_s and μ_d are the limiting static, and the dynamic (sliding) friction coefficients, respectively, β is the bowing position relative to the string length, Z is the characteristic wave resistance of the string, v_b represents the bow speed; F_Z is the bow force (often termed "bow pressure") and R the string-termination resistance (representing all losses).

These equations seem in general to be qualitatively correct, and have shown to be most valuable in evaluations of the dynamics of the bowed string. A main uncertainty lies in the difficulty to define an appropriate string termination resistance for a real instrument, and taking the torsional component of the string motion into account.

3. The build-up of friction forces during a bowed attack

When starting a bow stroke, the string player has in principle three options at hand:

1. starting the bow "from the air", i.e., with a certain bow speed, but from zero bow force
2. starting the bow "from the string", i.e., with some bow force, but from zero bow speed
3. starting the bow from zero bow speed and zero bow force.

It is the author's experience as a professional string teacher and player that violinists often utilise the first strategy when introducing the first note of a singing musical phrase, while their colleagues on the heavier string instruments (cello, double bass) more often prefer to initiate the attack with a certain string contact, also when aiming at gentle onsets. The reason for this most probably lies in the difference of transient duration, as any starting noise tends to last longer and thus be more disturbing on the lower-pitched instruments. For all string players, however, strategy (1) will unquestionably come to use when playing a true legato slur from one string to another. Experienced players of cello and double bass therefore often mask the inevitable multiple-slip noises resulting from this approach by letting the sound of the "old" string overlap while the sound of the "new" string is building up. This is simply a matter of changing the bow angle slowly. Within a singing phrase not involving string crossings, however, accomplished string players tend to keep the bow in good contact with the string between strokes, as any lifting would disturb the sonority and break up the musical stream. For this reason, string students spend much time practising inaudible bow changes, as well as clean onsets of separate tones, with the bow in full string contact. The present study is focused on what might be a good strategy for obtaining the Helmholtz motion, and thus a full sound as quickly as possible, when starting the stroke in the latter manner, i.e., "from the string".

In order to do so, we shall first pursue an option that is not available to the player: starting the bow stroke instantaneously, "switched on", with both bow speed and bow force at fixed nonzero values. We will do so simply because this draws the clearest picture of what sets the limits when trying to obtain periodic string releases. For the same reason, we shall start the analyses with the simplest possible bowed-string model.

During stick on a flexible string in a loss-free system, excited (in a single point) by a bow starting with the constant velocity v_0 at $t = 0^+$, the static friction force can be expressed as

$$f_{ST}(t) = \tag{2}$$
$$2Z\left\{v_0 - \left[-\frac{f_{ST}(t-\beta T) + f_{ST}(t-(1-\beta)T)}{2Z}\right]\right\},$$

where T is the fundamental period.

Here the expression within the square brackets describes the sum of waves returning to the bow after total reflection at the respective string terminations. (E.g., the term $-\beta T$ indicates a time delay on the string equal to $\beta 2L/c$, for waves propagating from bow to bridge to bow, where L is the string length, and c the wave propagation speed.) The two time lags, and the loops they make with respect to f_{ST} on the left side of the equality sign, accumulate the string's force/velocity history.

If $(1-\beta)$ is several times larger than β, the friction force, $f_{ST}(t)$, will take the value of $2Zv_0$ in the time interval $0^+ \le t < \beta T$, values of $4Zv_0$ and $6Zv_0$ respectively in the intervals $\beta T \le t < 2\beta T$ and $2\beta T \le t < 3\beta T$, and continue with this increment until the time $(1-\beta)T$, where an extra force step occurs. Figure 3 describes the situation. The friction force builds up quickly in steps until a slip occurs. The picture becomes particularly simple when $(1-\beta)$ and β have an integer ratio. Apart from discontinuity of the steps, the friction force is nearly proportional to the bow's displacement, resembling the reactive force of a compressed spring.

In the simulation plotted in Figure 3, a raise in the limiting static frictional force at the instant of capture (i.e., at the time βT after the release) was programmed in order to avoid further slips. After the single slip, waves returning to the bow on the bridge side experience a positive offset with magnitude equal to the relative velocity $(v_{\mathrm{bow}} - v_{\mathrm{string}})$ that was experienced during the slip itself, while on the nut side, returning waves display *superimposed discrete pulses* of the same magnitude, and width equal to βT.

For later analyses we shall need a linear function to approximate this force buildup before any slip has occurred. The discussion to follow will reveal that constant-speed bowing is not the most illuminating case to consider: If the bow is allowed to accelerate, new effects appear, and the value of acceleration has a critical influence on the string behaviour. With this in mind, equations (3) and (4) have been written in a form which allows uniform bow acceleration at rate a.

By smoothing the steps (see the fractions with corresponding lines drawn in Figure 3) we can estimate the friction force to be close to $f_{ST}(t)$, which we will define as our "function of static friction force":

$$f_{ST}(t) := 2Z\left[v_0 + \frac{t(at+2v_0)}{2T\beta(1-\beta)}\right], \tag{3}$$

where v_0 is the bow velocity (starting at $t = 0$) and a is the bow accelaration (starting at $t = 0$).

A description of the development of equation (3) is found in Appendix A3. The function of equation (3) constitutes the first one of two expressions that appear practical when the criteria for periodic string releases in the simple system are to be defined in section 5. The second function, which concerns the slip, expresses a negative friction force, superimposed on the static friction force

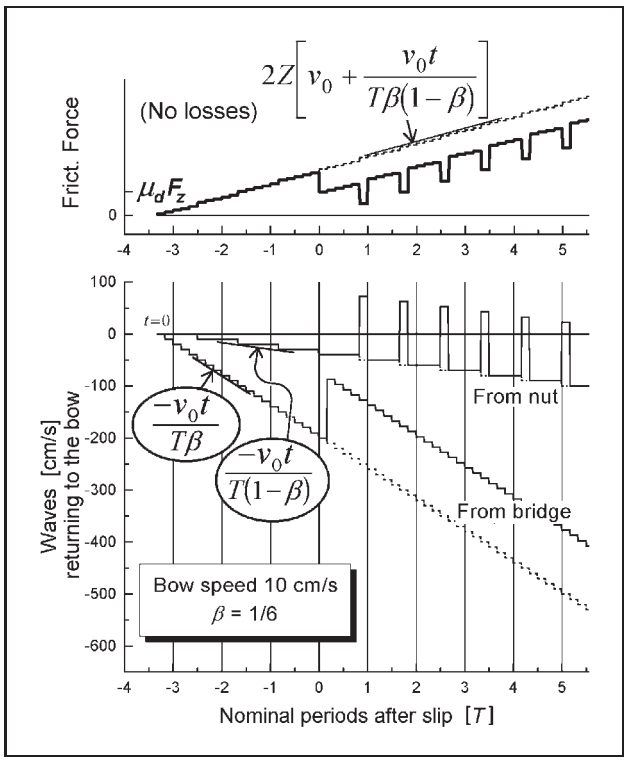

Figure 3. Friction-force build-up, and velocity waves returning to a bow with constant speed–one string flyback included. When a string is bowed with constant speed, returning waves build up in steps. A slip (i.e., a negative string velocity pulse) will be superimposed on these waves after having been reflected at the string terminations, but only as discrete pulses for the ones returning from the nut. In this simulation the limiting static frictional force was raised at capture (after βT), in order to see the effect of one slip only. Dotted lines indicate the situation without any slip ($\lambda_{BRG} = \lambda_{NUT} = 1$; friction characteristics: "hyperbolic").

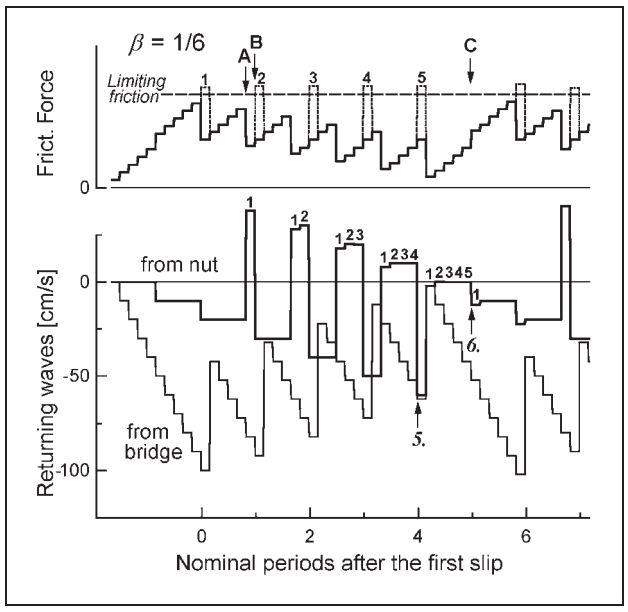

Figure 4. Friction force and wave build-up in a string bowed with a constant speed that gives periodic triggering over a few initial periods. Upper plot: The dashed lines indicate "potential friction force", i.e., the friction force that would have occurred if no slip took place at this instant. Lower plot: The (string-flyback) pulses stacking up after returning from the nut are indexed in order to trace their origin. The italic numbers 5. and 6. indicate sufficient and insufficient pulse heights, respectively ($\lambda_{BRG} = \lambda_{NUT} = 1$; friction characteristics: "hyperbolic").

defined above (confer the reductions in friction force and bridge-reflected velocity after the slip in Figure 3):

$$f_{SL}(t, \mu_d) \equiv F_Z \mu_d - f_{ST}(t). \tag{4}$$

With $F_Z \mu_d$ held constant over the entire slip, the magnitude of f_{SL} will by definition be increasing in the same interval. We will, however, let these functions rest for a while, and show a situation where the combination of constant bow speed and bow force provides regular slips, occurring in intervals equal to the fundamental period in the first part of the stroke. Given $1/\beta$ is an integer, the picture appears as described in Figure 4:

In Figure 4 the bow velocity has been chosen to provide regular periodic triggering for the first $1/\beta - 1$ (i.e., five) periods. The waves returning to the bow after reflections at the bridge and nut start out in the same way as they did in Figure 3. In Figure 4, however, we experience several successive slips, the reflections of which each time form a positive "offset" on the bridge side of the bow. These occur at times βT after each release, and have magnitudes equal to the relative slip velocity ($v_{\mathrm{bow}} - v_{\mathrm{string}}$). On the nut side the same reflected pulses stack up, one after the other, in a cyclic pattern of period $(1-\beta)T$, always with the reflected first-slip pulse in front. (Each pulse is indexed with respect to the slip number so that one can trace its origin.) What we have are two loops, one on the bridge side, one on the nut side, with periods βT and $(1-\beta)T$, respectively. After $1/\beta - 1$ (i.e., five) periods, the return of the first-slip pulse–$1/\beta$ times reflected at the nut–coincides with the time of the periodic release. This velocity pulse is now oriented in the bowing direction, and thus reduces the frictional force considerably at the moment the slip number $1/\beta$ (i.e., six) is due to be triggered.

In Figure 4, three time points are marked **A**, **B**, and **C**, respectively. These indicate critical moments during the creation of Helmholtz motion and largely constitutes the base on which the present analysis is founded:

At **A** (defined as $t_a = t_{rel} + (1-\beta)T$, where t_{rel} is the time of the first string release), the first friction-force maximum occurs after the initial slip. (With no losses and a constant bow speed, it actually occurs βT earlier, but holds the same value until **A**). This friction-force value must be no more than the limiting static frictional force if a premature triggering shall be avoided at this point. The force maximum at **A** consequently determines the *upper limit* for bow speed if regular periodic triggering of release shall be obtained. (Remember that each single force step is $2Zv_b$ high and βT wide.)

At **B** (defined as $t_b = t_{rel} + T$), where a second string release is supposed to take place in order to establish periodicity, the *potential* friction force *must surpass* the limiting static frictional force to trigger the slip. Correspond-

ingly, the limiting static frictional force determines the *minimum* bow speed at this point.

The slip-pulse "offsets" that were mentioned earlier are determined by the delta $\mu_s - \mu_d$, and give force reductions proportional to this difference.

Provided the bow speed is kept within the limits defined at $\mathbf{A}$ and $\mathbf{B}$, slips will be regularly spaced with intervals equal to the fundamental period until the next obstacle occurs at $\mathbf{C}$ (defined as $t_c = t_{rel} + (1/\beta - 1)T$). At this instant, the initial string-flyback pulse (indexed "1") – $1/\beta$ times reflected between the nut and the bow – coincides with the nominal time of periodic release. This largely cancels the pulse supposed to trigger slip number $1/\beta$ (see the arrows marked 5. and 6. in Figure 4, and compare the respective signals arriving from the nut.) Due to inappropriate potential frictional force, no release takes place at $\mathbf{C}$.

These three critical points in the bowed-string transient can be compared to the two critical points in the Raman/Schelleng analysis: In Figure 2, the friction force must be no more than $\mu_s F_Z$ at $\underline{\boldsymbol{A}}$. The same goes for the friction force at $\mathbf{A}$ of Figure 4. In Figure 2, the *potential* friction force *must be higher than* $\mu_s F_Z$ at $\underline{\boldsymbol{B}}$. The same is true for the potential friction force at both $\mathbf{B}$ and $\mathbf{C}$ of Figure 4. In fact, with a system without losses the (minimum) bow-speed requirement at $\mathbf{C}$ will always be higher than the (maximum) bow-speed requirement at $\mathbf{A}$, which excludes constant bow speed as a strategy for obtaining Helmholtz triggering in loss- free systems.

In Figure 4 it can also be seen that while waves returning from the bridge form descending steps, as they should in order to create a Helmholtz pattern similar to that of Figure 1, response from the nut side fails to shape the ascending counterpart.

4. Loss and bow acceleration

Figures 5 and 6 indicate two strategies that may remedy the triggering failure at time point $\mathbf{C}$:
(1) By introducing losses at the nut side, the magnitude of the initial pulse will diminish for each new reflection, thus reducing its cancelling potential after $1/\beta$ reflections. Figure 5 describes the situation. Notice: as long as the bow's impedance is infinite and there is no torsion present, the string sections on both sides of the bow can be considered separated.
(2) By accelerating the bow, magnitudes of the successive string flyback pulses will be increasing, which again will reduce the cancelling potential of the relatively smaller first pulse. Figure 6 shows the result.

In Figure 5 we notice how the losses at the nut make the history of the first slip diminish after each reflection there (see pulses indexed "1" at the lower panel). In Figure 6, there are no losses, but successive slip pulses are growing in magnitude due to the acceleration of the bow. In both examples a certain "stair-case building" takes place on the nut side as required for establishing the Helmholtz mode, although it fails in providing the appropriate slopes, yet.

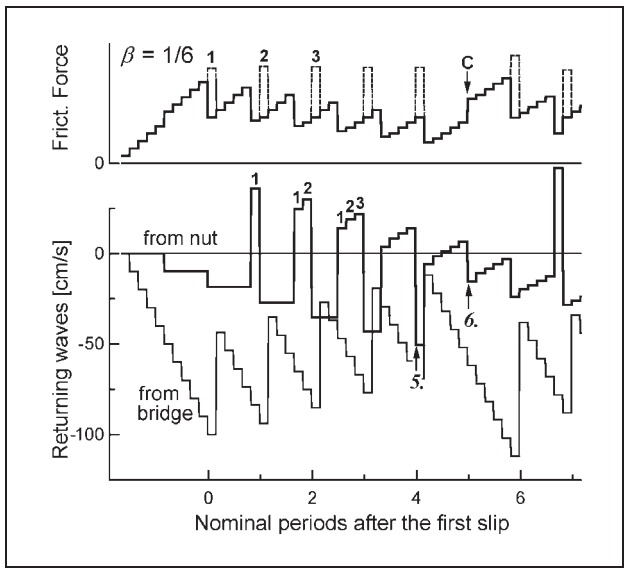

Figure 5. Friction force and wave build-up in a string bowed with constant speed and 5% loss at the nut. By introducing loss at the nut side, the waves returning from this end start to shape up as required for the Helmholtz motion. However, a 5% resistive loss (i.e., nut reflection coefficient, $\lambda_{NUT} = 0.95$) is still inadequate to provide regular triggering with the parameters chosen ($\lambda_{BRG} = 1$; friction characteristics: "hyperbolic").

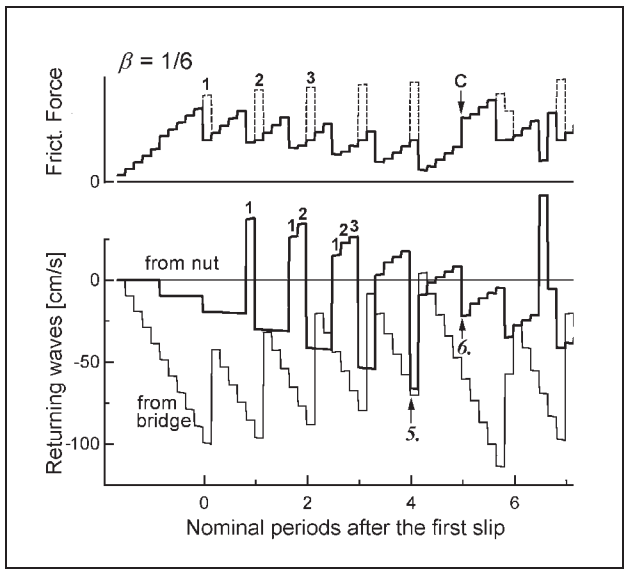

Figure 6. Friction force and wave build-up when the bow is given a small acceleration. By superimposing acceleration on the initial bow speed, waves returning from the nut start to shape up as required for the Helmholtz motion. Even greater acceleration would have ensured regular triggering ($\lambda_{BRG} = \lambda_{NUT} = 1$; friction characteristics: "hyperbolic").

Both strategies seem qualified to form adequate wave patterns, provided loss or acceleration of appropriate magnitude. Apparently there is not much to choose between them. But, of course, with the losses defined by the system, only bow acceleration remains as control parameter for the player.

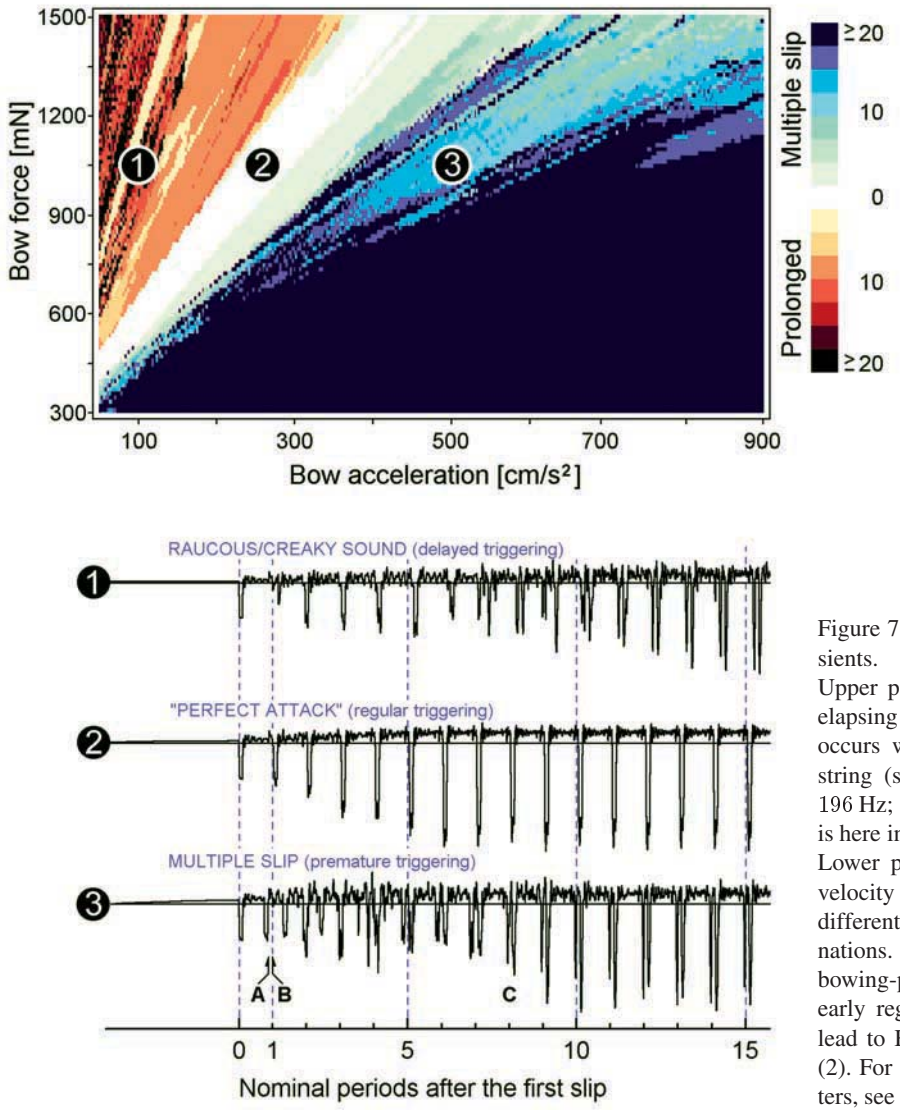

Figure 7. Categories of bowed-string transients.
Upper panel: number of nominal periods elapsing before regular periodic triggering occurs with a high-impedance violin G-string (set of 33000 simulations: $F_0 = 196$ Hz; $\beta = 1/9 = 0.11$). String torsion is here included.
Lower panel: selected waveforms (string velocity under the bow) resulting from different bow-force / acceleration combinations. Musicians mostly try to achieve bowing-parameter combinations that give early regular triggering and thus quickly lead to Helmholtz motion, i.e., waveform (2). For details on the simulation parameters, see string II of Figure 11.

5. Searching for bowing parameters that ensure periodic triggering

Guettler and Askenfelt [9] found that string players are very sensitive to the duration of non-periodic triggering in bowed violin attacks. "Neutral tone onsets" on an open G-string (196 Hz) were considered to be of unacceptable quality if the duration of multiple slips (or prolonged periods) exceeded 90 (50) milliseconds, or 18 (10) nominal periods. Dependent on the damping of the system, multiple slips will normally prevail for quite a few periods once encountered. String players therefore make an effort to steer clear of this, and most of them develop a remarkable skill in avoiding such noises where the music does not call for it. In the preparation of reference [9], where a total of 1694 violin attacks were classified by inspection of the string waveform, 44% were found to be "perfect" (defined as less than 5 ms elapsing before the occurrence of Helmholtz triggering). In that study two professional violin players were asked to perform excerpts from the violin literature without knowing the purpose of the study. Consequently they could be assumed to pay no more than normal attention to clean attacks.

A few successive "perfect attacks" in spiccato (record of string velocity) are furthermore demonstrated in Figure 6 of reference [10].

Figure 7 (lower panel) shows three typical string velocity waveforms resulting from different transient bowing parameters, as computed with a simulation model including string stiffness, torsion, bow compliance, and "plastic" friction characteristics (see Figure 11 for system details). In the white triangle of the upper plot of Figure 7, combinations of bow acceleration and bow force have produced "perfect attacks", like the one shown in waveform (2) below. At the upper left side of this triangle, one or more of the initial periods were prolonged, causing irregular string releases over a number of periods following (1). At the lower right side, multiple slips occurred quickly, as the bow was accelerating too much for holding the string stuck till the end of the first nominal period (3). It can fur-

thermore be seen from the string waveforms that example (1) failed at "**B**", while example (3) failed at "**A**", or just before that point of time.

Our task shall be to calculate the bowing-parameter combination able to produce the shortest transient, i.e., a "white triangle"–if not for this complex string model, at least for the simple model analysed in the previous section.

We shall be searching for equations that comply with the requirements at the time points **A** (i.e. $t_a = t_{rel} + T(1-\beta)$), **B** (i.e. $t_b = t_{rel} + T$), and **C** (i.e. $t_c = t_{rel} + T(1/\beta - 1)$) as shown in Figure 4. That is: the (potential) friction force must *surpass* the limiting static value at time points **B** and **C**, whereas its value must be *no more than* the limiting value at point **A**, as mentioned earlier. Since a first string release will take place when $f(t) \geq F_Z\mu_s$, we can calculate the approximate time t_{rel} to be:

$$t_{rel} \approx \sqrt{\frac{v_0^2}{a^2} + \frac{T\beta(1-\beta)(F_Z\mu_s/Z - 2v_0)}{a}} - \frac{v_0}{a}, \qquad (5)$$

($a > 0$, $v_0 < F_Z\mu_s/2Z$). By separating the *constant-velocity* bow from the *accelerating* bow, we get simpler expressions (the equations are indexed a or b in order to indicate solutions for bow *velocity* or *acceleration*, respectively):

$$t_{rel} \approx T\beta(1-\beta)\left(\frac{F_Z\mu_s}{2v_0 Z} - 1\right), \qquad (5a)$$

($a = 0$, $v_0 < F_Z\mu_s/2Z$) and

$$t_{rel} \approx \sqrt{\frac{T\beta(1-\beta)F_Z\mu_s}{aZ}}, \qquad (5b)$$

($a > 0$, $v_0 = 0$). Thus, just after the moment when the string slips for the first time the resulting friction force may be expressed, utilising the functions of equations (3) and (4):

$$\begin{aligned}\hat{f}(t_{rel}^+) &= f_{ST}[t_{rel}] + f_{SL}[t_{rel}, \mu_d] \\ &= F_Z\mu_s + f_{SL}[t_{rel}, \mu_d] = F_Z\mu_d.\end{aligned}$$

Having determined the time and friction force of (i.e., just after) the first release, the *relative velocity*, $v_{\text{relative}} = v_{\text{string}} - v_{\text{bow}}$, is easily found:

$$v_{\text{relative}}(t_{rel}^+) = \frac{F_Z\mu_d - \hat{f}(t_{rel}^-)}{2Z} = \frac{F_Z(\mu_d - \mu_s)}{2Z}.$$

By use of the two functions of equations (3) and (4), we can furthermore conveniently formulate the approximate requirements of a loss-free system for the time points **A** and **B**, respectively, provided $1/\beta$ is an integer:

$$f_{ST}[t_{rel} + T(1-\beta)] + f_{SL}[t_{rel} + T\beta, \mu_d] \leq F_Z\mu_s, \quad (6)$$

and $$f_{ST}[t_{rel} + T] + f_{SL}[t_{rel}, \mu_d] > F_Z\mu_s. \qquad (7)$$

The left-hand sides of equations (6) and (7) represents "static friction force" and "potential friction force", respectively.

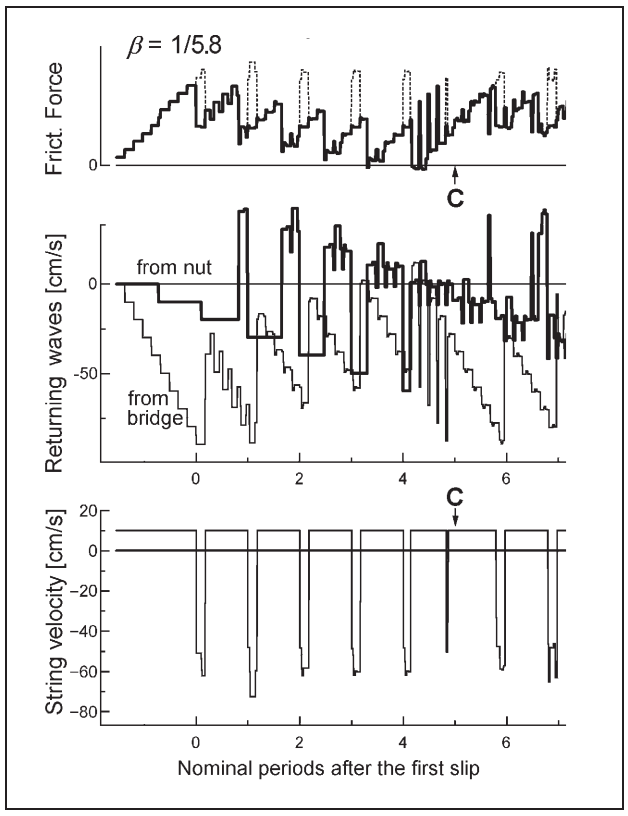

Figure 8. Example of friction force and wave build-up for a string bowed with constant speed in a non-integer-ratio position. When exciting the string in a non-integer-ratio position, the patterns of frictional force and waves returning to the bow become more complex and hence less suitable for simple algebraic analysis. As in Figure 4, the periodic triggering fails at **C** (in this case not $t_{rel} + (1/\beta - 1)T$, but $t_{rel} + 5T$), where the 6th periodic triggering should have occurred. A minor premature slip can, however, be observed just before that time ($\beta = 1/5.8$; $\lambda_{BRG} = \lambda_{NUT} = 1$; friction characteristics: "hyperbolic"; no string torsion).

Whenever a slip pulse is created during the transient, it will split and propagate in both directions away from the bow. On both sides the pulses are locked in between the bow and the string termination as long as the bow's impedance is much higher than the characteristic impedance of the string (see Figure 3). For each reflection (at the nut, bridge, or bow) the slip pulse will be turned around 180 degrees, implying that every time it is heading toward the bow, it has the same $\partial y/\partial t$ orientation as the bow itself. Provided the pulse on the bridge side has a width equal to βT, it hence represents an uninterrupted (but not necessarily constant) reduction of the friction force, as was shown in Figure 3. In equations (6) and (7), the "slip function", $f_{SL}[t, \mu_d]$, thus refer to the "history" of the initial slip which took place in the time interval t_{rel} to $t_{rel} + \beta T$. After this (superimposed negative) force pulse has been $1/\beta - 2$ times reflected between the bridge and the bow, as for equation (6), its last part arrives at the bow at the time point **A**, giving a force reduction (relative to $f_{ST}[t_{rel} + (1-\beta)T]$) equal to what took

place *at the end of the original slip interval*. In equation (7), the same slip pulse has been $1/\beta$ times reflected when the history of its front arrives at the bow at the time of the supposed release, **B**, giving a force reduction (relative to $f_{ST}[t_{rel}+T]$) equal to what took place *at the beginning of the original slip interval*. Since the magnitude of the slip pulse is by definition increasing over the slipping interval (confer equations 4 and 3), this distinction is necessary.

For the same reason we restrict our analysis to cases where $1/\beta$ is an integer: to avoid the complication of keeping track of, calculating, and summing a number of instantaneous velocity values derived at different phases of a series of nonrectangular slip pulses. Figure 8 shows the effect of excitation in a non-integer-ratio position for the simple case of constant bow speed in a loss-free system. Although the main features of Figure 4 are still recognisable, details are here considerably more complicated. In a practical situation, where the width of the bow-hair ribbon covers a certain string length, such (local) fluctuations might, however, be less observable.

Solved for a constant bow velocity, v_0, equations (6) and (7) give together:

$$\underbrace{\beta(1-\beta)F_Z\frac{(\mu_s-\mu_d)}{2Z}}_{\mathbf{B}} < v_0 \leq \underbrace{\frac{\beta(1-\beta)}{(1-2\beta)}F_Z\frac{(\mu_s-\mu_d)}{2Z}}_{\mathbf{A}} \quad (8a)$$

($a=0$, $\beta<0.5$)[1] and, solved for a constant bow acceleration, a:

$$\underbrace{\beta(1-\beta)F_Z\frac{3\mu_s-\mu_d-2\sqrt{2\mu_s^2-\mu_s\mu_d}}{TZ}}_{\mathbf{B}} < a \leq \beta(1-\beta)F_Z\Big[(3-4\beta)\mu_s-\mu_d \underbrace{-2\sqrt{(1-2\beta)\big(2(1-\beta)\mu_s^2-\mu_s\mu_d\big)}\Big]\Big[(1-2\beta)TZ\Big]^{-1}}_{\mathbf{A}} \quad (8b)$$

($v_0=0$, $\beta<0.5$). We notice here that in contrast to Schelleng's equation for steady state, i.e., equation (1) (and our own equation concerning constant bow velocity, equation 8a), equation (8b) presents bow acceleration as a function of the string's fundamental frequency, which is equal to $1/T$. This implies longer-lasting transients for amplitude build-up at low pitches. When played on the same string, acceleration is proportional to frequency. Notice also that TZ is equal to twice the mass of the vibrating string, so there exists an inverse proportionality between the mass of the string and a.

At point **C**–provided $1/\beta$ is an integer and that previous slipping intervals have been regular–the condition for slip can be expressed as the solution to the equation

$$f_{ST}[t_{rel}+T(1/\beta-1)]+\lambda^{1/\beta}f_{SL}[t_{rel},\mu_{d1}] + f_{SL}[t_{rel}+T(1/\beta-2),\mu_{d2}] > F_Z\mu_s, \quad (9)$$

where λ is the reflection coefficient at the nut. For μ_{d1} and μ_{d2}, see the text below.

The left-hand side of equation (9) represents "potential friction force".

The term $f_{SL}[t_{rel}+T(1/\beta-2),\mu_{d2}]$ of equation (9) sums up the history of all previous slips (or rather their fronts) for the bridge side, while the term $f_{SL}[t_{rel},\mu_{d1}]$ reflects the history of the front of the first slip alone, having travelled as a discrete pulse back and forth $1/\beta$ times on the nut side. The expression $\lambda^{1/\beta}$ requires a comment: With losses, a slip pulse reflected once at the nut will have its shape changed, dependent on the frequency-phase response of the string-termination reflection (including string losses). Hence, iterative filtering does not imply logarithmic reduction of a fixed waveform unless the reflection is purely resistive. In the present case, the expression should be interpreted as "$\lambda^{1/\beta}$ is the total coefficient of $1/\beta$ nut reflections, with concern to the *front part* of the original slip pulse (i.e., the release)". As long as the string is excited in an integer-ratio position, it is this part of the pulse that has the potential of cancelling a $1/\beta$-th release at point **C**. (For a further discussion on this, see Appendix A4.) From the equations (10a) and (10b) below, we can see how the loss on the nut side has substantial impact on the minimum required velocity (or acceleration). Loss on the bridge side does not play the same role, but would be important for smoothing the force build-up during stick.

With an accelerating bow, the relative speed, $|v_{\text{relative}}|$, increases from slip to slip during most of the transient (see e.g. Figures 15 and 16). As we move out on the hyperbolic or a similar friction curve, μ_d diminishes. Since the effect of this reduction is likely to be quite noticeable at **C**, the coefficients of equation (9) are indexed, referring to the friction parameter operating at the time given as the first independent variable of the function in question. This is particularly important for low-magnitude F_Z and/or a. When solving equation (9) we get the following requirements at point **C**:

$$v_0 > \beta(1-\beta)F_Z\frac{(1+\lambda^{1/\beta})(\mu_s-\mu_d)}{2Z}, \quad (10a)$$

and

$$a > \beta^2(1-\beta)F_Z\Big[(1-1.5\beta)(C+\lambda^{1/\beta})(\mu_s-\mu_{d1})+\beta\mu_s - \sqrt{(2\beta-3\beta^2)(C+\lambda^{1/\beta})(\mu_s^2-\mu_s\mu_{d1})+\beta^2\mu_s^2}\Big] \cdot\Big[2(1-1.5\beta)^2TZ\Big]^{-1}, \quad (10b)$$

where $C=(\mu_s-\mu_{d2})/(\mu_s-\mu_{d1})$.

[1] Notice: When estimating constant bow speed in a loss-free system, not including string torsion,one might – rather than linearising – base the last expression directly on the step function, which gives

$$v_0 \leq \underbrace{\beta F_Z\frac{(\mu_s-\mu_d)}{2Z}}_{\mathbf{A}}, \quad (a=0,\ \beta<0.5).$$

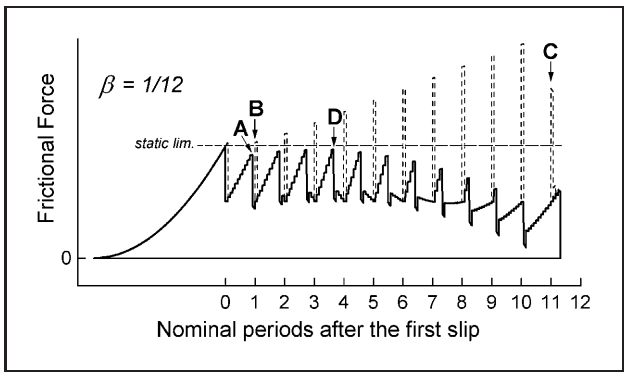

Figure 9. Rising friction-force peaks resulting from bow acceleration in combination with a small β. Bow acceleration may create static friction force peaks with an envelope rising after the initial period. The peak at point **D** is higher than the one at point **A**. Equations (6) and (8b) are hence inadequate for predicting a maximum bow speed in this case. Short-dash lines: "potential friction force" ($\lambda_{BRG} = \lambda_{NUT} = 1$; friction characteristics: "hyperbolic").

In addition to the obstacles at time points **A** through **C**, there is, however, a fourth phenomenon that potentially limits our range of acceptable acceleration: For small β, the envelope of the static-friction force peaks may be growing after the initial period–from the first restriction point, **A**, to an apex a few periods later (see Figure 9, and Appendix A5). (As we could notice in Figures 4 and 5: with a constant bow speed the static friction-force maxima were diminishing from period to period during the $1/\beta$ initial periods.)

With μ_d held constant, the highest force peak will typically be found in the static-friction interval of period number $1/(3\beta)$. It is therefore feasible to estimate a second acceleration limit with respect to that point, **D** (defined as $t_d = t_{rel} + T(1-\beta)/(3\beta)$), in order to avoid a premature slip here. The requirement at time point **D** thus becomes:

$$f_{ST}[t_{rel} + T(1-\beta)/(3\beta)] + f_{SL}[t_{rel} + T(1/(3\beta) - 1 + \beta), \mu_d] \leq F_Z \mu_s, \quad (11)$$

which solved for a gives an equation that in its full form reads

$$a \leq 9\beta^2(1-\beta)F_Z\Big[(2-3\beta^2)\mu_s - (2-4\beta+3\beta^2)\mu_d - 2\sqrt{(2\beta-3\beta^2)\big[(2-2\beta)\mu_s^2 - (2-4\beta+3\beta^2)\mu_s\mu_d\big]}\Big] \cdot \Big[(8-44\beta+104\beta^2-132\beta^3+90\beta^4-27\beta^5)TZ\Big]^{-1}. \quad (12)$$

The left-hand side of equation (11) represents "static friction force".

6. Verification of accuracy of the equations

Simulations were used to verify the accuracy of the above equations with concern to the simple bowed-string model. In a parameter space of bow acceleration: 50 to 900 cm/s^2 (abscissa), and bow force: 0 to 1000 mN (ordinate), more than 15000 simulations were performed per plot (other parameters: $T = 5.0$ ms; $Z_{TRV} = 0.22$ kg/s; $\lambda = 1$; friction characteristics: hyperbolic with $\mu_s = 1.0$; $\mu_d(10\text{cm/s}) = 0.75$; $\mu_d(\text{asymptotic}) = 0.5$). Each simulation, which lasted twelve nominal periods after the first slip, was categorised and given a grey-tone pixel according to the number of nominal periods elapsing before periodic triggering occurred. The resulting plots are found in the left-hand panels of Figure 10. These plots show the responses at six different β, all of which had integer ratios, and thus qualifying for the use of the equation set.

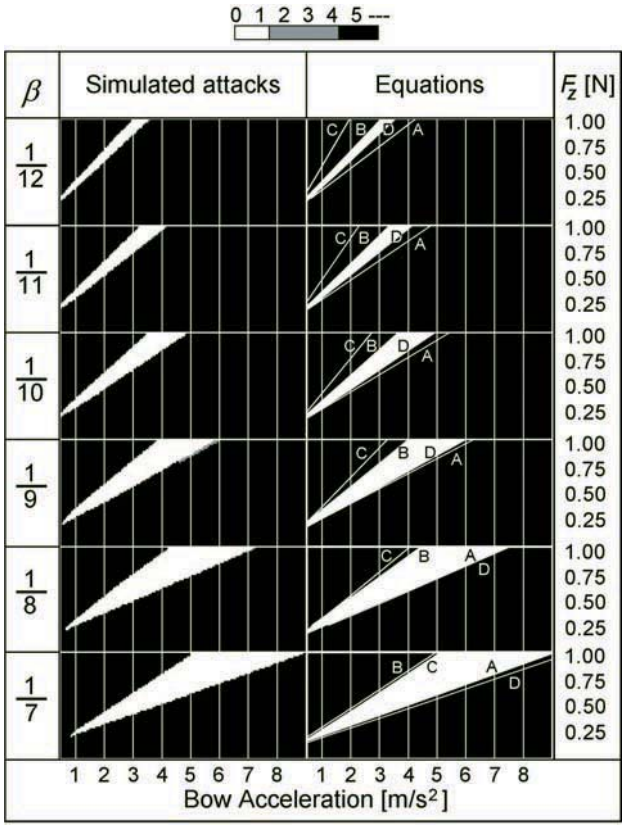

Figure 10. Comparison between simulated attacks and the four limiting equations (number of nominal periods elapsing before regular periodic triggering). Panels to the left are describing simulation sets of different β. White colour is indicating regular triggering from the very beginning ("perfect attacks"). In the panels to the right, limits set by equations (8b), (10b), and (12)–referring to the time points **A** through **D**–are marked A, B, C, and D, respectively: In order to achieve "perfect attacks", the bow acceleration should be kept lower than both A and D, and *higher* than B and C. Notice that for small β, B and D give the strongest requirements, while for large β the situation is reversed, i.e., C and A giving the most narrow limits. Exactly at which β these exchanges take place depends on the μ_d/μ_s ratio.

In the right-hand panels of Figure 10, predictions of the equations are plotted. The functions are labelled A through D in accordance with time points they refer to: A = equation (8b), right side; B = equation (8b), left side; C = equation (10b), and D = equation (12). To avoid "subjective selection" of friction coefficients, to which the equa-

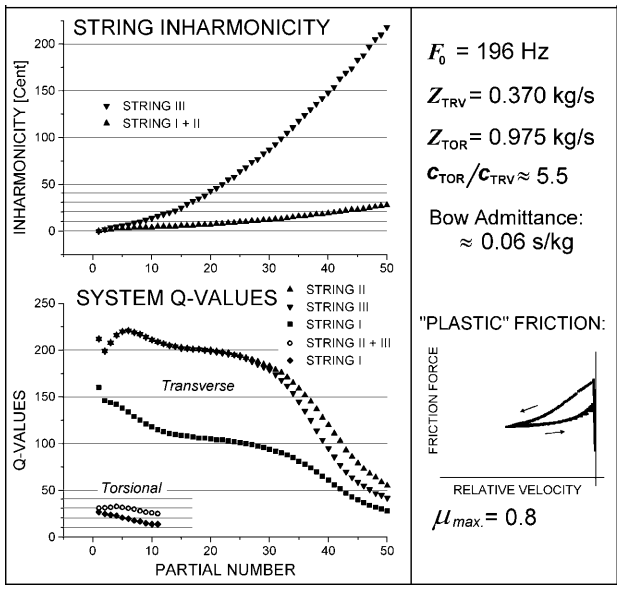

Figure 11. String-parameter overview. String I has moderate stiffness and the lowest Q-values. String II has the same moderate stiffness combined with higher Q-values. String III has very high stiffness combined with the higher Q-values. The spectral envelopes of the reflection functions of strings II and III are identical, the difference in their Q-values are all due to differences in their inharmonicity, i.e., in their partial frequencies. The inharmonicity is given in cents defined by $C = 1200\log(F_n/nF_0)/\log 2$, where F_n is the frequency of the nth partial.

tions are highly sensitive, the following procedure was used: For each parameter space, three simulations were performed (with F_Z values of 0.25, 0.5 and 1.0 N, respectively), whereafter the friction coefficients of the *simulations* were derived from the appropriate phases of the attacks by the computer, and inter/extrapolated for the chosen range of F_Z.

In general, Figure 10 shows simulations and predictions in good correlation–particularly where the frictional characteristics are not extrapolated. The white triangles ("perfect attacks") do not extend all the way down to the origin as one might have expected from inspecting the equations. The reason for this lies in the choice of a hyperbolic friction characteristic: The friction-coefficient delta (i.e., $\mu_s - \mu_d(t_{rel}^+)$)–determined by the friction curve's intersections with the string's load line–decreases as F_Z decreases, and vanishes when $F_Z \leq 88$ mN. The hyperbolic curve itself, which is uniquely defined through three coordinates, is of the form $\mu = c_1 + c_2/(v_{\text{relative}} + c_3)$, where c_1–c_3 are constants.

7. The problem of including torsion in the equations

Since the transverse system described by equation (3) closely resembles that of a spring with stiffness $2Z_{TRV}/[\beta(1-\beta)T]$, the torsional system might with the same precision and limitations be described as $2Z_{TOR}/[\beta(1-\beta)\zeta T]$, where Z_{TRV} and Z_{TOR} are the transverse and torsional wave resistances, respectively, and ζ is the ratio between transverse and torsional propagation speeds. The "parallel reactance" of these two systems can thus be expressed as

$$\frac{2TZ'}{\beta(1-\beta)T}, \quad \text{where} \quad Z' = \frac{T_{TOR}Z_{TRV}}{T_{TOR}+\zeta Z_{TRV}}. \quad (13)$$

In principle, equation (3) may hence be adjusted for torsional admittance–and torsional waves returning to the bow–by replacing its wave-impedance term Z with the modified Z'. (Notice: Z' is not the familiar "parallel impedance", $Z_{TRV}Z_{TOR}/(Z_{TRV}+Z_{TOR})$, which remains valid as half the impulse impedance of the string surface).

However, while inserting Z' in equation (3) gives a fair estimate of the force build-up before the first string release, the "ringing" caused by torsional waves as response to a slip during the transient makes equations (6) through (12) quite unsuitable as predictors of the acoustical outcome. This ringing, which is caused by mutual transformations between transverse and torsional pulses, is described in Figures 2 through 6 of reference [11], and the related text. Such ringing varies with the torsional Q-values, as well as with different combinations of β and ζ, the analysis of which will have to wait for another study.

8. Simulations with more complex models

Although the equations discussed are unsuitable for predicting the acoustical outcome of more complex systems, the patterns they outline for simpler systems can still to some extent be recognised in the more advanced ones, as shall be shown. Simulations were performed for three complex bowed-string models. In all cases the string impedances were: $Z_{TRV} = 0.370$ kg/s and $Z_{TOR} = 0.975$ kg/s (comparable to a "heavy" steel violin G-string [12]), $c_{TOR}/c_{TRV} = 1/\zeta \approx 5.5$, and bow admittance ≈ 0.06 s/kg above 100 Hz (derived from [13]). "Plastic" friction characteristic was used (see Appendix A4 and [7]. The example trajectory shown in Figure 11 is result of a steady-state Helmholtz motion at $\beta = 1/6$, $v_{bow} = 10$ cm/s, and $F_Z = 0.7$ N, simulated with String II). Two different string-stiffness parameters were combined with two different reflection-functions' spectra in order to characterise three different string qualities (labelled String I–III). String stiffness was obtained by use of the Airy function, as suggested by Woodhouse in [4]. Figure 11 show the simulation parameters in terms of impedances, inharmonicity and Q-values, while the results of the respective simulations are shown in Figure 12.

In the plots of Figure 12, the picture is noticeably more complicated than for the simulations with the simple model of Figure 10. Nonetheless, a certain underlying structure seems to shine through and is most clearly seen for String I.

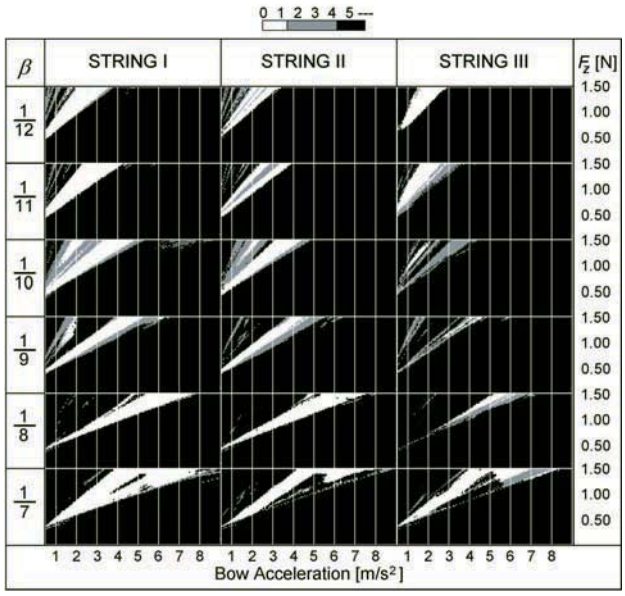

Figure 12. Number of nominal periods elapsing before regular periodic triggering occurs for three different bowed-string systems. Triangular patterns can still be recognised–particularly for String I and II, although not with the same consistency as in Figure 10. While the abscissas are identical in Figures 10 and 12, the ordinate has been increased by 50% in Figure 12 to compensate for differences in the friction characteristics, etc.

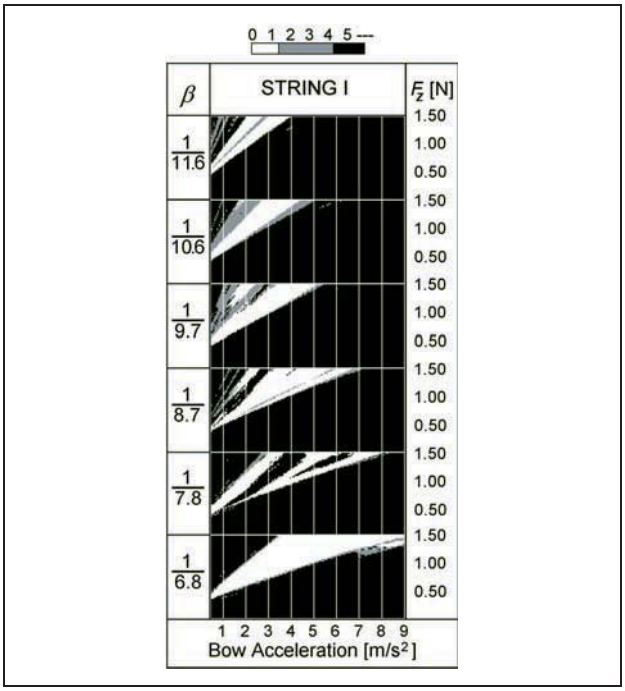

Figure 13. Number of nominal periods elapsing before regular periodic triggering occurs for String I bowed in a non-integer-ratio position. When lowering the Q-values and utilising the plastic friction model, attacks "bowed" in non-integer-ratio positions produce plots quite similar to the ones produced with the bow in integer-ratio positions (compare to Figure 12). The system parameters are all equal to those given for String I of Figures 11 and 12.

The choice of damping parameters has not yet been discussed. Woodhouse and Loach [14] tested the average torsional Q-value of a steel cello D-string to be 34, while nylon and gut strings measured 46 and 20, respectively. For transverse modes, an average Q-value of 500 has been utilised by some authors [15]. There is, however, a good reason for lowering these values somewhat when examining attack responses, as done in this paper. The reported values originate from measurements on open (un-fingered) strings. Every string player knows that bowed attacks are much harder to perform on open strings than on fingered ones. For this reason bass and cello players often pluck open strings lightly with their left hand during bowed attacks. In any string instrument a fingered string decays much more rapidly than an open one. One may hence presume that the fingered string exhibits significantly lower Q-values, and that this represents the normal situation for the string player.

As stressed on several occasions already, the present analysis is entirely based on integer-ratio positions of the bow. The reason for this lies not solely in the computational simplicity. In general, a set of non-integer-ratio β would fail to produce "favourable" force-acceleration triangles with the same consistency as the integer-ratio ones–at least when the system is loss-free. However, when the Q-values are lowered to (presumably) reasonable levels, the structure of these triangular areas can easily be recognised. Figure 13 shows examples with the same system as used for String I of Figures 11 and 12.

In Figure 14, the parameters of Strings I–III are used once more, this time with bow strokes of constant velocity and force. To add realism, the bow was allowed half a nominal period for acceleration. One striking difference between the plots of Figures 12 and 14 is that in the latter very few "perfect" attacks were produced for $\beta > 1/9$. With these larger β values the periodic triggering usually failed (cancelled by the nut-reflected initial slip pulse) at time point **C**–not surprisingly. It should, however, be mentioned that when string torsion is included, reflections at the bow introduce additional losses, which to some extend reduces the cancelling potential of this pulse.

Figures 15 and 16 shows examples of "perfect" attacks for two different systems: Figure 15 displays the onset leading to the steady-state Helmholtz motion of Figure 1, while Figure 16 gives the corresponding onset for the more complex model of String II. In both simulations β is equal to 1/6. Notice the build-up of waves returning to the bow on the nut side in each case. The basic features are quite similar. Notice also how the flyback velocity in both cases appears reduced at slip number 6, i.e. at time point **C**, where interference with the remains of the initial slip pulse–$1/\beta$ times reflected on the nut side of the bow–takes place.

One may conclude from comparing Figures 15 and 16 that the major structure of wave buildup in the string's transverse plane is not extremely sensitive to torsion, string stiffness, or differences in friction characteristics

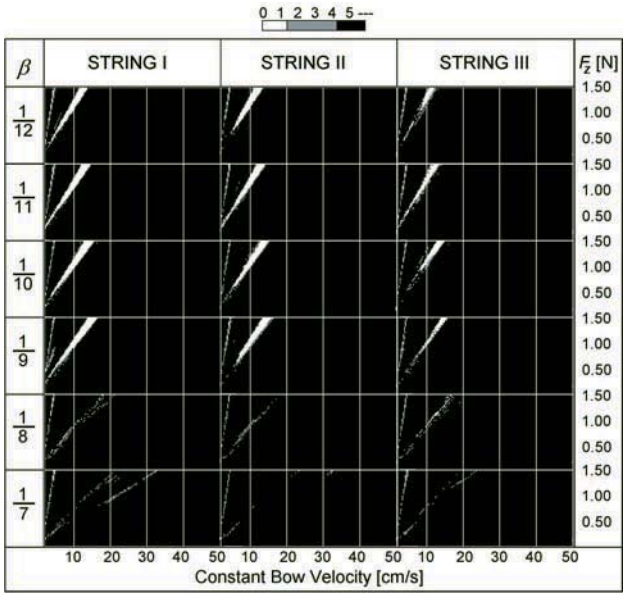

Figure 14. Number of periods elapsing before regular triggering occurs when starting the bow with constant speed and force. Losses are adequate for making "perfect" attacks as long as $\beta \leq 1/9$.

during the creation of Helmholtz motion–at least when the string is bowed in an integer-ratio position.

Schelleng suggested a slightly raised bow force at the beginning of a note or rapid crescendo in order to provide the energy to be stored in the string. From the simulation of Figure 16 it is possible to derive that in order to maintain the periodic triggering with the bow-velocity parameters programmed, the limiting static frictional force should decrease no more than ca 0.3% per period during the first seven nominal periods, and thereafter no more than 0.9% per period for the following 8. The post-attack reduction of bow force must thus be performed with some care, even after the final bow velocity has been reached.

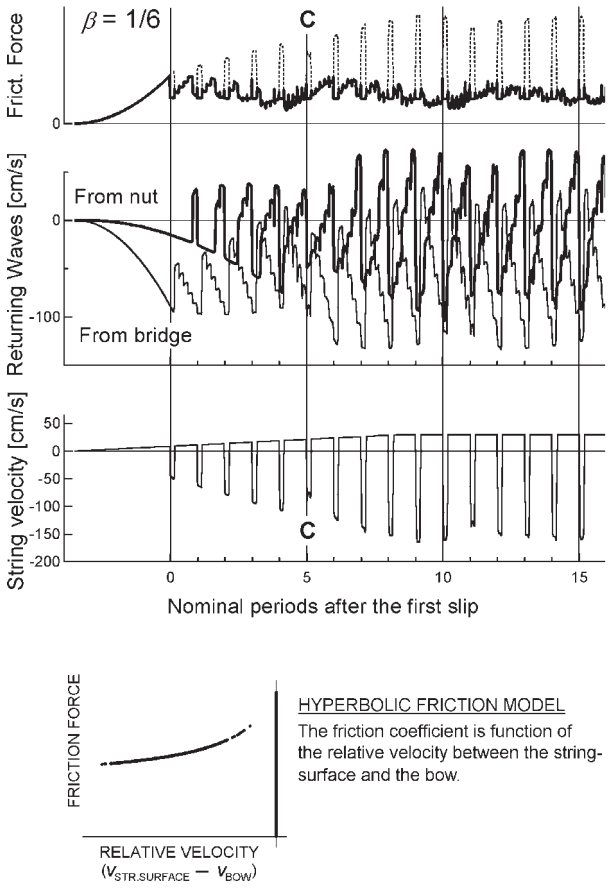

Figure 15. Build-up to Helmholtz motion with simple bow-string models. Top panel: Friction force during a bowed transient with regularly spaced slip pulses. Dotted lines: "potential friction force". Upper middle panel: Waves (including "echoes" of successive slip pulses) returning to the bow after reflections at the nut and bridge, respectively. Notice how the reflections from the nut stack up in a periodic pattern with pulses of increasing heights. Lower middle panel: Because there is no torsion, the string is following the bow perfectly during stick. Bottom panel: The "hyperbolic" friction model is quite simple.

9. Conclusions

Some characteristic features of bowed-string onsets leading to the Helmholtz motion have been presented. In the (post transient) Helmholtz motion, using the analysis of d'Alembert's solution to the wave equation, waves travelling toward the bow from each side can be seen to form nearly symmetrical patterns during the stick interval. Arriving from the bridge side, adjacent pulses form steps increasingly opposing the movement of the bow. Simultaneously arriving from the nut side, steps go more and more in the bow's direction. During slip, waves from both bridge and nut have their maxima in terms of opposition to the bow velocity, which is the reason why the release normally takes place. The creation of this pattern requires a history of a number of slip pulses stacking up with increasing magnitudes on the nut side during the transient. Apparently, this would only be the case when the bow is given some initial acceleration, and/or: if losses of the system provide sufficient magnitude reduction in slip pulses several times reflected between the bow and the nut. Hence, for the player, bow acceleration is a most important means for reaching the wanted combination of bow force and string amplitude without introducing undesirable onset noise.

Most of the analyses of this paper were done with bowed-string models of the simplest kind, i.e., loss-free systems, or systems with small losses concentrated at the string terminations. In order to acquire intelligible equations, an unsophisticated friction model was used, derived from a hyperbolic friction-coefficient curve descending with increasing relative bow-string surface velocity. Based on this set-up, four equations were suggested, which– considering a flexible string with fairly rigid terminations, excited by a bow of infinite impedance in an integer-ratio position–give the approximate range for bow acceleration (or speed) capable of producing a slip-stick triggering pattern with intervals equal to the fundamental period of the string over a number of initial periods. Although the equa-

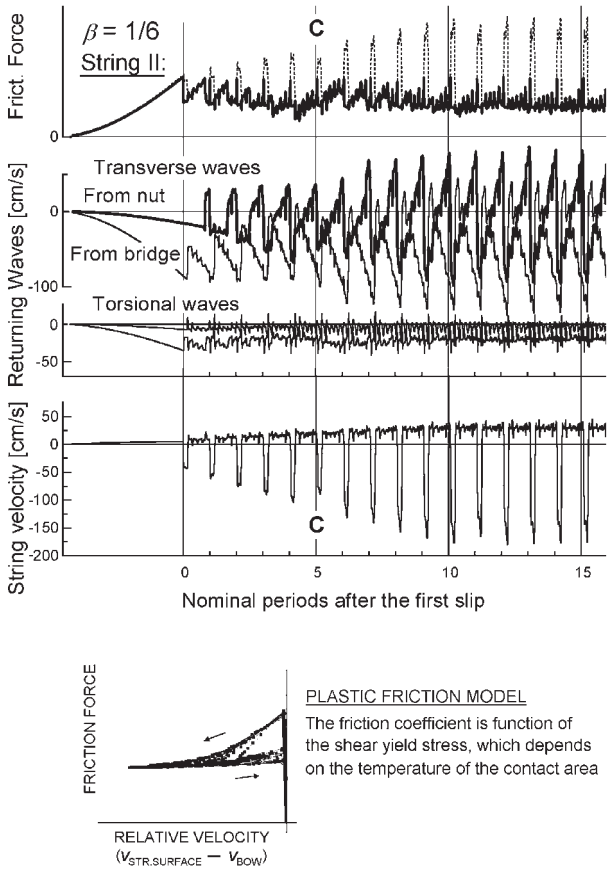

Figure 16. Build-up to Helmholtz motion with advanced bow-string models. A "perfect" attack transient simulated with more advanced string and friction models (equal to those used for String II of Figures 7, 12, 13, and 14). Even when bow compliance and string torsion are included, the transverse wave pattern does not differ substantially from that shown in Figure 15, simulated with the simpler models. The bottom panel shows the (plastic) friction force trajectories of the present simulation.

tions themselves are not directly transferable to more realistic systems, the pattern they describe seems to provide some insight in the conditions for development of the Helmholtz motion, even in more complex models.

Coda A string player can control the bow's acceleration not only by the arm movement, but also by the firmness of the bow hold and wrist. Many players have found this to be particularly effective when attacking the string close to the bridge, where the bow's acceleration should be kept smooth in the first part of the transient in order to avoid noise of extra slips, caused by a rapidly changing frictional resistance.

Appendix

A1. D'Alembert's wave equation

D'Alembert's solution to the wave equation reads

$$y(x,t) = y_+(x - ct) + y_-(x + ct), \tag{A1}$$

where the signs indexing y denotes the direction of wave propagation, and c its speed. Furthermore,

$$\frac{\partial y}{\partial x} = y'_+ + y'_-, \quad \frac{1}{c}\frac{\partial y}{\partial t} = -y'_+ + y'_-, \tag{A2}$$

and

$$y'_+ = \frac{1}{2}\left(\frac{\partial y}{\partial x} - \frac{1}{c}\frac{\partial y}{\partial t}\right), \quad y'_- = \frac{1}{2}\left(\frac{\partial y}{\partial x} + \frac{1}{c}\frac{\partial y}{\partial t}\right). \tag{A3}$$

A2. "Potential frictional force"

The frictional force between a noncompliant bow and the string during the static intervals may be expressed through the following equation, which can be derived from [16], equations (B13) and (B14):

$$F_{ST} = 2Z_{CMB}\left[v_b(t) - \sum_{i=1}^{4} v_i(t)\right], \tag{A4}$$

where Z_{CMB} is the combined wave impedance of the string, i.e. for a string with rotational freedom $Z_{TRV}Z_{TOR}/(Z_{TRV} + Z_{TOR})$, otherwise Z_{TRV}; $v_b(t)$ is the velocity of the bow, $v_i(t)$ denotes the partial wave (i.e. $\partial y_i/\partial t$) arriving at the bow. $v_1(t)$ and $v_2(t)$ are *transverse* signals propagating away from the nut and the bridge, respectively, $v_3(t)$ and $v_4(t)$ are *torsional* signals propagating away from the nut and the bridge.

The sum of the four partial signals (i.e., velocities) gives the surface velocity the string would have taken at the point of bowing without friction. It is convenient to refer to $F_{ST}(t)$ as "potential frictional force" regardless of whether the friction be static or not.

A3. System impulse response–Development of equation (3)

Let us consider a system where the impulse response of a flexible string with one reflecting termination (at $x = 0$), excited in a point ($x = \beta L$), is expressed through a causal Green's function $g(t)$, comparable to the method employed in [17] and [3]. The string velocity at βL is:

$$v(t) = \int_0^\infty g(\tau) f(t - \tau)\, \mathrm{d}\tau, \tag{A5}$$

where $g(t)$ is the Green's function of the system, and $f(t)$ is the friction force at the point of excitation.

$g(t)$ comprises here a Dirac delta and a reflection function, h_0, that includes a delay equal to the time required for a wave to propagate from the bow to the bridge and back:

$$g(t) = \frac{\delta(t) + h_0}{2Z}, \tag{A6}$$

where

$$h_0 = \frac{Z - R}{Z + R}\delta(t - t_1), \tag{A7}$$

and $Z = m'c$ is the transverse wave resistance, R the resistance of the bridge, m' is the mass of the string per unit length, c is the wave propagation speed, and $t_1 = 2\beta L/c$.

If $Z \ll R$, h_0 may be approximated as $h_0 = -\delta(t-t_1)$, in which case we get

$$g(t) = \frac{\delta(t) - \delta(t-t_1)}{2Z}, \tag{A8}$$

and

$$v(t) = \frac{1}{2Z}\int_0^\infty \big[\delta(\tau) - \delta(\tau - t_1)\big] f(t-\tau)\,\mathrm{d}\tau. \tag{A9}$$

We are interested in knowing what the force function must be in order to maintain a constant string and bow velocity v_0, starting at $t = 0$. Using the Laplace transform, we get

$$\begin{aligned} V(s) &= \frac{v_0}{s}, \qquad G(s) = \frac{1 - \mathrm{e}^{-t_1 s}}{2Z}, \\ F(s) &= \frac{V(s)}{G(s)} = 2Zv_0 \frac{1}{s(1 - \mathrm{e}^{-t_1 s})} \\ &= Zv_0 \frac{1 + \coth(t_1 s/2)}{s}. \end{aligned} \tag{A10}$$

When returned to the time domain, equation (A10) gives the force function we know from earlier, which builds up in steps of magnitude $2Zv_0$, at time intervals of t_1:

$$f(t) = 2Zv_0 \sum_{n=0}^{k} \theta(t - nt_1), \tag{A11}$$

where $k = \mathrm{Floor}(t/t_1)$, Floor(*val.*) is the largest integer $\leq$ *val.*, and $\theta(t)$ the unit step.

For our transient analyses, however, we need a smooth function to describe $f(t)$ during "stick", so we choose

$$\hat{f}(t) = v_0\left[2Z + \frac{2Zt}{t_1}\right] = v_0\left[2Z + \frac{2Zt}{2\beta L/c}\right], \tag{A12}$$

which outlines the magnitude maxima of equation (A11), i.e., it gives the correct value each time $t/T\beta$ is an integer. The fraction inside the square bracket expresses a virtual stiffness. By repeating the procedure described by equations (A5) through (A11) for the other string termination with a reflection function, $h_L = -\delta[t - 2(1-\beta)L/c]$, and combining the two in a single expression, we get

$$\hat{f}(t) = v_0\left[2Z + \frac{2Zt}{2\beta L/c} + \frac{2Zt}{2(1-\beta)L/c}\right], \tag{A13}$$

which, by replacing $2L/c$ with T (i.e. the fundamental period) gives

$$\hat{f}(t) = v_0\left[2Z + \frac{2Zt}{\beta(1-\beta)T}\right]. \tag{A14}$$

Once more the fraction inside the square bracket can (for our purposes) be thought of as an expression of stiffness– this as partial impedance of a string with two fixed ends, dynamically excited a point βL somewhere between the two.

In a system starting from rest with an acceleration, a, at $t > 0$, the first term inside the square brackets of equations (A12) through (A14) is omitted since $v_{bow}(0) = 0$, and the friction force consequently zero. That leaves us with an expression for "virtual dynamic impedance", quite simple, linear, and suitable for estimating static friction-force build-up under an accelerating bow of infinite impedance:

$$\overline{Z} = \frac{2Z}{\beta(1-\beta)T}, \tag{A15}$$

which gives

$$\hat{f}(t) \simeq \overline{Z}\frac{at^2}{2} = \frac{Zat^2}{\beta(1-\beta)T}. \tag{A16}$$

For comparison, the correct force function is

$$f(t) = at * 2Z\left[\delta(t) + \sum_{n=1}^{k}\delta(t-nt_1) + \sum_{m=1}^{j}\delta(t-mt_2)\right], \tag{A17}$$

where $k = \mathrm{Floor}(t/t_1)$, $j = \mathrm{Floor}(t/t_2)$, and the asterisk denotes convolution.

The discrepancy between equations (A16) and (A17) is small for small β, and diminishes as t increases. For $\beta = 1/5$ the maximum error is less than 0.31% when $t > 3T$, and less than 0.15% when $t > 5T$, which is more than sufficient for our purpose. Whenever $t/T\beta$ and $t/T(1-\beta)$ are both integers, equation (A16) gives the value without error.

Notice also that the term at in equation (A17) might have been replaced by any arbitrary velocity function $v(t)$:

$$f(t) = v(t) * 2Z\left[\delta(t) + \sum_{n=1}^{k}\delta(t-nt_1) + \sum_{m=1}^{j}\delta(t-mt_2)\right]. \tag{A18}$$

A4. On the potential string-release cancellation at C

Figure A1 illustrates the problem of determining the value $\lambda^{1/\beta}$ of equation (9). Depending on the nature of the reflection function(s), the initial-slip pulse arriving from the nut at the time $t_c = t_{rel} + T(1/\beta - 1)$ might take different shapes. With $1/\beta$ being an integer, it is the front of the ($1/\beta$ times reflected) pulse that has the potential of cancelling the string release at this instant. For a reflection function where the ratio between frequency and logarithmic decrement is constant (as for constant-Q systems) the situation appears as in Figure A1, provided no phase shift takes place.

While the damped pulse has its maximum at its middle, its front does not nearly reach this magnitude (As a thumb

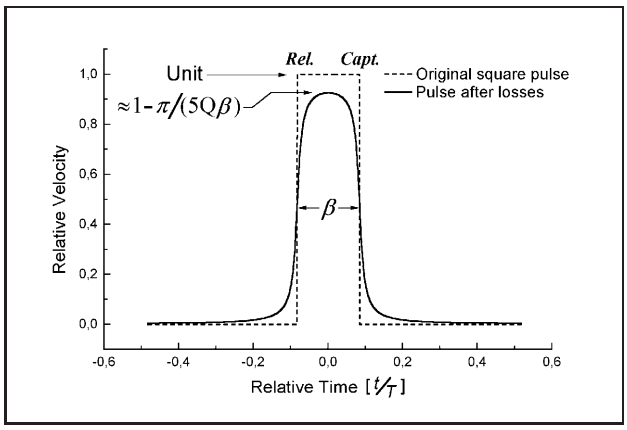

Figure A1. Example of square pulse after frequency-dependent loss. When passing a constant-Q filter, a rectangular pulse is "smeared" out. The actual Q-values of the filter used for this figure was 30 for all frequencies while the phase response was zero. The abscissa gives time relative to the fundamental period.

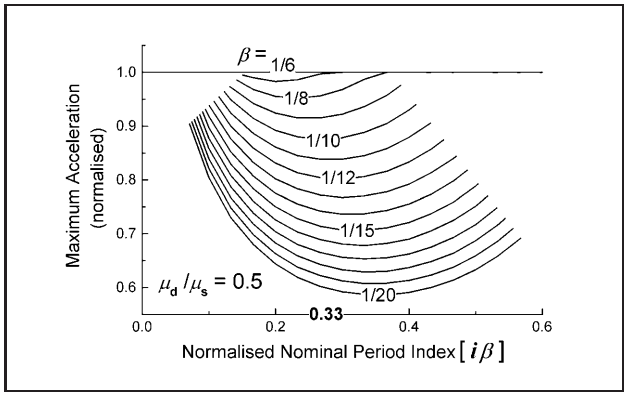

Figure A2. Maximum acceptable acceleration at $\boldsymbol{D}$ compared to ditto at $\boldsymbol{A}$. Which one of the two being the more restrictive depends primarily on β, but also to some extend on the ratio μ_d/μ_s. In most practical cases where the equation at $\boldsymbol{D}$ sets the most conservative limits, the limiting force peak is found in the period number $\approx 1/(3\beta)$ after the first release, giving $i\beta = 0.33$.

rule–giving an error less than 0.5%–the normalised pulse-height decrement is approximately equal to $\pi/(5Q\beta)$ for $\beta \geq 1/30$ in combination with constant Q-values ≥ 100). The cancelling potential of a damped pulse with respect to a "fresh" one of opposite orientation depends on the importance of the "spikes" remaining at both ends. In the case of the plastic friction model, a certain time is needed for the temperature build-up necessary for a string release of significant flyback velocity.

The friction coefficient of the plastic model follows the equation [7]

$$\mu = \frac{A k_y(\mathrm{Temp})}{N}\mathrm{sgn}(v), \tag{A19}$$

where A represents the contact area, N the normal force, $k_y(\mathrm{Temp})$ the shear yield stress (function of temperature), Temp is the temperature and v the relative velocity (bow hair – string surface).

The temperature rises as function of frictional energy and decays due to natural heat flow to the environment. In practice, A seems to be growing with N, nearly proportionally. Only limited information has yet emerged on the characteristics of k_y [7, 18]. For the simulations in the present study the following friction function was used: The friction coefficient μ as function of lasting relative speed approaches a hyperbolic curve at a rate determined by a heat-flow half time of 40 μs. The long-term curve (which is uniquely defined by three coordinates, see section 6) has the following characteristic points at $\mu(v_{rel}, t)$: $\mu(0, \infty) = 0.800$; $\mu(20\,\mathrm{cm/s}, \infty) = 0.575$; $\mu(\infty, \infty) = 0.350$.

A5. On the restrictions at A and D

With an accelerating bow, the friction force shows distinct apexes at each sticking interval during the first part of the transient (see Figure 9). These occur at time points $iT(1-\beta)$ after the first release, starting with **A** at $i = 1$, where i is indexing the nominal periods after t_{rel}. Considering these force maxima individually, the maximum acceptable bow acceleration of period number i is the solution to

$$f_{ST}[t_{rel} + iT(1-\beta)] + f_{SL}[t_{rel} + T(i-1+\beta), \mu_d] \leq F_Z \mu_s, \tag{A20}$$

which, with respect to acceleration, gives

$$a_{\max}(i) = \frac{F_Z \mu_s}{TZ}\Bigg[\beta(1-\beta) \cdot \Big[1-\beta+2i-3\beta i + \frac{\mu_d}{\mu_s}(1-\beta-2i+\beta i) - 2\sqrt{(1-\beta+\beta i)\Big[2i-2\beta i + \frac{\mu_d}{\mu_s}(1-\beta-2i+\beta i)\Big]}\Big] \Big[(1-\beta-\beta i)(1-\beta-2i+\beta i)^2\Big]^{-1}. \tag{A21}$$

We see that equation (6) is only a particular case of equation (A20), in which $i = 1$.

Figure A2 gives the ratio $a_{\max}(i)/a_{\max}(1)$, that is, $a_{\max}(i)$ divided by the right side of equation (8b), or, $a_{\max}(i)$ normalised to the acceleration limit caused by the force apex at **A**. The lowest acceptable maximum acceleration depends not only on i, however, but also on β and the fraction μ_d/μ_s. Figure A2 shows how this restriction varies as function (here shown continuous) of the product $i\beta$, for a ratio $\mu_d/\mu_s = 0.5$. It is seen that for $\beta \geq 1/6$, the apex at **A** is the most restricting feature. For smaller β, an apex near $t = t_{rel} + [1/(3\beta)]T(1-\beta)$ is the most restricting one (i.e., when $i \approx 1/(3\beta)$, or $i\beta \approx 0.33$). For practical reasons equations (11) and (12) were hence chosen with the fixed value $i = 1/(3\beta)$, although the true function varies slightly with both β and the μ_d/μ_s ratio.

Acknowledgement

The author wants to express his gratitude to one of the anonymous reviewers who contributed substantially with

constructive ideas on the presentation of this rather tangled subject.

References

[1] J. C. Schelleng: Pressure on the bowed string. Catgut Acoust. Soc. Newsletter **13** (1970) 24–27.

[2] J. C. Schelleng: The bowed string and the player. J. Acoust. Soc. Am. **53** (1973) 26–41.

[3] R. Schumacher: Self-sustained oscillations of the bowed string. Acustica **43** (1979) 109–120.

[4] J. Woodhouse: On the playability of violins. Part I: Reflection functions. Acustica **78** (1993) 125–136.

[5] R. Pitteroff: Contact mechanics of the bowed string. PhD dissertation, University of Cambridge, 1995.

[6] K. Guettler, A. Askenfelt: Relation between bow resonances and the spectrum of a bowed string. Proc. International Symposium of Music Acoustics '95, Edinburgh, 1995, 231–237.

[7] J. H. Smith, J. Woodhouse: The tribology of rosin. Journal of the Mechanics and Physics of Solids **48** (2000) 1633–1681.

[8] C. V. Raman: On the mechanical theory of the vibrations of bowed strings and of musical instruments of the violin family, with experimental verification of the results. Part I. Indian Assoc. for the Cultivation of Science, Bull **15** (1918) 1–158.

[9] K. Guettler, A. Askenfelt: Acceptance limits for the duration of pre-Helmholtz transient in bowed string attacks. J. Acoust. Soc. Am. **101** (1997) 2903–2913.

[10] K. Guettler, A. Askenfelt: On the kinematics of spiccato and ricochet bowing. Catgut Acoust. Soc. J. (Series II) **3** (1998) 9–15.

[11] K. Guettler: Wave analysis of a string bowed to anomalous low frequencies. Catgut Acoust. Soc. J. (Series II) **2** (1994) 8–14.

[12] N. Pickering: Physical properties of violin strings. Catgut Acoust. Soc. J. **44** (1985) 6–8.

[13] A. Askenfelt: Observations on the violin bow and the interaction with the string. Proc. International Symposium of Music Acoustics (ISMA'95), Edinburgh, 1995, 197–212.

[14] J. Woodhouse, A. R. Loach: Torsional behaviour of cello strings. Acustica **85** (1999) 734–740.

[15] S. Serafin et al.: An investigation of the impact of torsion waves and friction characteristics on the playability of virtual bowed strings. Proc. 1999 IEEE Workshop on Applications of Signal Processing to Audio and Acoustics, 1999.

[16] M. E. McIntyre, R. T. Schumacher, J. Woodhouse: On the oscillations of musical instruments. J. Acoust. Soc. Am. **74** (1983) 1325–1345.

[17] M. E. McIntyre, J. Woodhouse: On the fundamentals of bowed-string dynamics. Acustica **43** (1979) 93–108.

[18] J. Woodhouse, R. T. Schumacher, S. Garoff: Reconstruction of bowing point friction in a bowed string. J. Acoust. Soc. Am. **108** (2000) 357–368.